

# Influence of minor hydrocarbon seepage on sulfur cycling in marine subsurface sediments

hat gelöscht: and its significance for hydrocarbon reservoir detection...

Ellen Schnabel<sup>1</sup>, Aurèle Vuillemin<sup>1</sup>, Cédric C. Laczny<sup>2</sup>, Benoit J. Kunath<sup>2</sup>, André R. Soares<sup>3</sup>, Rolando Di Primio<sup>4</sup>, Jens Kallmeyer<sup>1\*</sup> and the PROSPECTOMICS Consortium<sup>†</sup>

<sup>1</sup>GFZ German Research Centre for Geosciences, Section Geomicrobiology, Telegrafenberg, 14473 Potsdam, Germany

<sup>2</sup>Luxembourg Centre for Systems Biomedicine, University of Luxembourg, Esch-sur-Alzette, Luxembourg

<sup>3</sup>Environmental Metagenomics, Research Center One Health Ruhr of the University Alliance Ruhr, Faculty of Chemistry, University of Duisburg-Essen, Essen, Germany.

<sup>4</sup>AkerBP, 1366 Lysaker, Norway

<sup>†</sup><https://www.prospectomics.eu/>

<sup>15</sup> \*A full list of authors and their affiliations appears at the end of the paper.

*\*Corresponding author*

Jens Kallmeyer, GFZ German Research Centre for Geosciences, Section Geomicrobiology, Telegrafenberg, 14473 Potsdam, Germany, email: [kallm@gfz-potsdam.de](mailto:kallm@gfz-potsdam.de)

20

**Abstract.** All hydrocarbon (HC) reservoirs leak to some extent. When small quantities of HCs escape offshore reservoirs and migrate through overlying organic-poor marine sediments towards the surface, these HCs are often completely metabolized by [microorganisms](#) before reaching the sediment-water interface. However, [these](#) inconspicuous HC fluxes still [influence](#) the geochemistry of [surrounding](#) [sediments](#) and [potentially stimulate metabolic](#) activity [by](#) microbial populations in shallow subsurface environments.

25

In this study, we [examined](#) how localized HC seepage affects microbial sulfate reduction in organic-poor [sediments](#) from the SW Barents Sea, [focusing](#) on three [sampling](#) areas overlying known HC deposits and two [pristine seabed reference areas](#). The analysis of 50 gravity cores revealed significant variability in the predicted [sulfate depletion depth](#), ranging from 3 to 12 m below the seafloor. [We](#) observed nearly linear

30

hat gelöscht: microbial activity

hat gelöscht: affect

hat gelöscht: the

hat gelöscht: sediment, thereby exerting a subtle influence on the composition

hat gelöscht: of

hat gelöscht: ¶

hat gelöscht: investigated

hat gelöscht: sediment

hat gelöscht: . We focused

hat gelöscht: reference areas of

hat gelöscht: for comparison.

hat gelöscht: depth of

hat gelöscht: across sampling sites

hat gelöscht: Although we

pore water sulfate and alkalinity profiles, alongside low rates of sulfate reduction ( $\text{pmol} \times \text{cm}^3 \times \text{d}^{-1}$ ). Metagenomic and metatranscriptomic data indicated metabolic potential and activity towards sulfate reduction and anaerobic oxidation of methane (AOM). Expression of functional marker genes (*aprAB*, *dsrAB*, *mcrA*) revealed metabolic activities by sulfate-reducing Desulfobacterota and methanotrophic ANME-1 archaea sustained by HC traces in the sediment. Further, in concomitance to AOM processes, we found that archaea amongst the class Lokiarchaeia and Thoarchaeia were expressing genes involved in sulfur reduction (*hydB*, *hydG*).

- hat gelöscht: we measured and modeled
- hat gelöscht: ( $\text{pmol} \times \text{cm}^3 \times \text{d}^{-1}$ )
- hat gelöscht: on functional marker genes supported microbial turnover associated with active processes of
- hat gelöscht: ). Marker genes for taxonomy (i.e. SSU rRNA, *rpoD*), sulfate reduction (i.e.
- hat gelöscht: *aprAB*), methanogenesis and methanotrophy (i.e.
- hat gelöscht: revealed
- hat gelöscht: a consortium of
- hat gelöscht: bacteria
- hat gelöscht: , capable of harnessing energy for cell division (i.e. *ftsAZ*) from
- hat gelöscht: diffusing through

55 Overall, our study demonstrates that the gradient in pore water geochemistry, the rates of sulfate reduction processes, and the genetic features of microbial populations actively involved in sulfate-driven AOM processes are all affected by inconspicuous HC seepage. This slight HC seepage resulted in sulfate depletion at shallower depth and produced concomitant biogeochemical signatures in the shallow subsurface that enable the inference of deeply buried reservoirs.

## 60 1. Introduction

All hydrocarbon (HC) reservoirs leak to some degree (Hunt, 1995; Yergin, 2009; Heggland, 1998), with over 80 % of all seeps occurring directly above the reservoirs (Ciotoli et al., 2020). While large leakages result in conspicuous manifestations at the seafloor, (e.g. Cramm et al., 2021), minor seeps usually remain invisible at the sediment-water interface (SWI). Still, sediment geochemistry and microbiology in the vicinity of inconspicuous seepage sites may be altered by HC fluxes (Rasheed et al., 2013; Abrams, 2020). Slight geochemical changes are common in the direct surroundings of HC reservoirs and overlying sediments, yet distal manifestations also occur. As seepage propagates further upwards, traces of HCs sometimes reach the seabed (Abrams, 2020; Joye, 2020), but are often overlooked.

- hat gelöscht: (Ciotoli et al., 2020)
- hat gelöscht: . (
- hat gelöscht: ).

70 HC seepage triggers both geological and microbiological processes, changing physicochemical properties, such as sediment porosity, mineral and pore water composition, as well as microbial community composition and activity (Abrams, 2020; Hvoslef et al., 1996; Joye, 2020). Likewise, methane-containing pore fluids alter the sediment porosity and compressibility (Jang et al., 2018) that are traceable in the acquisition of seismic profiles (Rovere et al., 2020), and potentially result in changes in the sediment geochemical properties, e.g. clay texture, organic matter (OM) reactivity, metal content (Chen et al., 2023). HC influx will also alter pore water geochemistry and pH, promoting ion exchange reactions, dissolution, precipitation and structural conversion of minerals (Jiang, 2012). As a consequence, specific

- hat gelöscht: (
- hat gelöscht: ).

95 trace metals and metalloids (e.g. Cr, Cu, As, Se, Sb) that can be metabolized by specific microorganisms (Raab and Feldmann, 2003) tend to become enriched in the sediment pore water at seepage sites (Rasheed et al., 2013; Guseva et al., 2021). Finally, most offshore sediments are composed of pelagic deposits, i.e. clays, silts or biogenic oozes, containing only low amounts of bioavailable OM that becomes increasingly recalcitrant with depth of burial (Middelburg, 2018). Thus, the influx of HCs in such sedimentary systems  
100 represents an additional source of electron donors, providing chemical energy for microorganisms and potentially fueling various metabolic processes. The metabolic potential to break down and assimilate HCs has been identified in a large number of microorganisms, e.g. reviewed in Joye (2020), whose activities may induce concomitant effects in the pore water, organic and mineral fraction of the sediment (Kim et al., 2004).

hat gelöscht:

hat gelöscht: is

hat gelöscht: necessary

105 The quantitatively most important anaerobic OM degradation process in marine sediment is sulfate reduction (Jørgensen, 1982). Due to its abundance in seawater, sulfate diffuses into the sediment pore water where it is used as an electron acceptor by sulfate-reducing microorganisms composed of sulfate reducing bacteria and ANME (Knittel et al., 2018; Widdel et al., 2010). Sulfate reduction (SR) can be divided into two main pathways, namely organoclastic and methanotrophic SR. The respective overall reactions are:

hat gelöscht: (Widdel et al., 2010).

110 Organoclastic SR:  $2 \text{CH}_2\text{O} + \text{SO}_4^{2-} \longrightarrow 2 \text{HCO}_3^- + \text{H}_2\text{S}$  (Equation 1)

hat gelöscht:

Methanotrophic SR:  $\text{CH}_4 + \text{SO}_4^{2-} \longrightarrow \text{HS}^- + \text{HCO}_3^- + \text{H}_2\text{O}$  (Equation 2)

Due to the abundance of easily biodegradable OM and sulfate close to the sediment-water interface, organoclastic SR normally prevails in anaerobic OM degradation within the uppermost part of the sediment column, leading to a decrease in sulfate concentration. Methanotrophic SR becomes  
115 predominant only when biogenic or thermogenic methane diffusing from deeper sediments reaches the zone where sulfate is still available but approaches depletion (Martens and Berner, 1974). The narrow zone where both methane and sulfate are available is referred to as the sulfate-methane transition zone (SMTZ). Within the SMTZ, mainly methane, and potentially also other OM compounds (Beulig et al., 2019; Jørgensen et al., 2019b), are oxidized by microorganisms while sulfate is reduced (Equation 2).

120 Thus, the respective methane and sulfate fluxes exert control on the depth of the SMTZ (Borowski et al., 1996, 1999; Jørgensen and Kasten, 2006), which, under steady-state conditions, is usually a reflection of methanogenesis rates (Henrichs and Reeburgh, 1987) or fluxes of thermogenic methane (Hu et al., 2017). However, the SMTZ is highly dynamic and responds relatively rapidly (i.e. within decades) to shifts in pore water geochemistry (Sultan et al., 2016; Hong et al., 2016). Thus, microbially active subseafloor sediments exhibit significant variability in the depth of the SMTZ across different oceans, from 1 to 10

of meters on the continental shelf (Egger et al., 2018). [On the continental slope, the SMTZ can be down to 100 m below seafloor \(mbsf\) in extreme cases](#) (Nunoura et al., 2009), [but is usually not deeper than 25 mbsf](#).

**hat gelöscht:** down to ca. 100 m along

**hat gelöscht:** .

The subsurface biosphere hosts phylogenetically diverse and metabolically active microbial communities (Parkes et al., 2014; D'Hondt et al., 2004). Their metabolic activity depends mainly on biogeochemical cycling of nitrogen, phosphate and sulfur. At HC seepage sites, microbial communities are well-defined in terms of taxonomy and highly specialized in terms of metabolic functions, and are referred to as "seep biomes" (Ruff et al., 2015). [It has been known for many decades that methanogenic hydrocarbon degradation is carried out jointly by bacteria and archaea in underground hydrocarbon reservoirs. New studies suggest that \*Candidatus methanoliparum\* may be able to independently degrade long-chain alkanes and produce methane](#) (Wegener et al., 2022; Zhou et al., 2021; Zhang et al., 2024). Seep biomes show spatial heterogeneity, but are distinct from non-seep environments (Pop Ristova et al., 2015). The reported key microbial guilds include methane and oil oxidizers, sulfate reducers, and nitrogen fixers. [Taxa found near HC seeps involve members of the bacterial phyla \*Desulfobacterota\* and \*Chloroflexota\*](#) that can respectively use simple and halogenated HCs as electron acceptors (Kleindienst et al., 2014; Zhang et al., 2023), whereas archaeal groups, like the ANME or [Asgardarchaeota](#), consume methane or make use of HCs or sulfur compounds (Firrincieli et al., 2021; Macleod et al., 2019).

**hat gelöscht:** h

**hat gelöscht:** These

**hat gelöscht:** Sulfate reducers potentially

**hat gelöscht:** Asgard archaea

Our study aims to determine in what ways inconspicuous HC seepage modifies the diversity and activity of anaerobic methanotrophs and sulfate-reducing bacteria in surface sediments of the SW Barents Sea. We hypothesize that minor HC seepage influences pore water geochemical properties, even in near-surface sediment, and that resident microbial communities respond quickly in terms of composition and activity to the geochemical alteration of their habitats.

For this, we collected 40 gravity cores from areas affected by light, inconspicuous HC seepage from underlying HC reservoirs (i.e. HC-affected sites) and 10 gravity cores from [seabed](#) areas without seepage from reservoirs (i.e. reference sites). We combine detailed analyses of pore water sulfate and alkalinity with potential and modeled sulfate reduction rates, dissolved methane (CH<sub>4</sub>) and carbon dioxide (CO<sub>2</sub>) concentrations, and supplement them with metagenomic (i.e. total DNA) and metatranscriptomic (i.e. total RNA) data [on taxonomic and functional marker genes in order to trace metabolic activity by microbial sulfate-reducing consortia in their geochemical context](#).

**hat gelöscht:** of selected samples

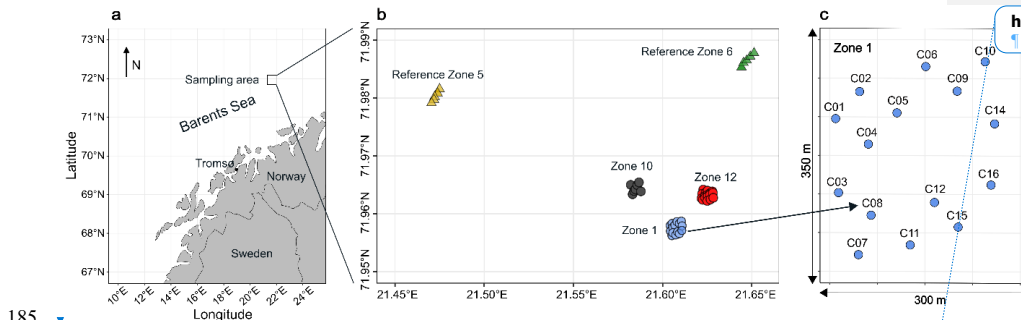
## 2. Material and methods

### 2.1 Geological context of the Barents Sea, sampling sites

The Barents Sea is an epicontinental shelf sea surrounded by the marginal Norwegian Sea to the southwest, the Arctic Ocean to the north and the Russian island Novaya Zemlya to the east (Fig. 1a). Since its formation during the Caledonian orogeny (i.e. 490-390 Ma), the Barents Sea Basin experienced several phases of uplift and subsidence, with subsequent tilting and erosion. These geologic events resulted in the characteristic structure of the Barents Sea in the form of a succession of structural highs and basins (Gabielsen et al., 1990; Larssen et al., 2002).

175 HC exploration in the Barents Sea has a history stretching back several decades (Doré, 1995; Johansen et al., 1993). The sediments have been characterized in numerous studies, e.g. Sættem et al. (1991), Elverhoi and Solheim (1983), and are mainly composed of organic-poor silty clays (Knies and Martinez, 2009; Nickel et al., 2013) originating from eroded sedimentary and igneous rocks.

During an expedition to the southern Loppa High region of the Barents Sea (Fig. 1a) from October 29<sup>th</sup> to November 8<sup>th</sup> 2021, we collected 50 gravity cores (up to 3 m in length) sediment at about 350 m water depth at three areas with known underlying HC reservoirs (i.e. Zone 1, Zone 10, Zone 12) and at two reference areas (i.e. Ref 5, Ref 6) without underlying HC reservoirs (Fig. 1b), labelled thereafter HC-affected sites and reference sites, respectively. The cores were subsampled for sediment and pore water on board the research vessel.



185 **Figure 1. Sampling locations.** (a) Map of the Norwegian coast. The square marks the sampling area. (b) Fifty cores were retrieved from three HC-affected sites (Zone 1, Zone 10, Zone 12) and two reference sites (Ref 5, Ref 6). (c) Each site was sampled in a grid of cores, Zone 1 is enlarged here as an example.

hat gelöscht: Hydrocarbon

hat gelöscht: (

hat gelöscht: )

hat gelöscht: )

hat gelöscht: positive

hat gelöscht: †

hat gelöscht: positive zones

hat gelöscht: zones

hat gelöscht: zone

hat gelöscht: here we show

200 The missing samples in the middle are due to the increased occurrence of dropstones in this area, preventing the deployment of a gravity corer.

hat gelöscht: center were

hat gelöscht: hardgrounds

hat gelöscht: ,

## 2.2 Pore water and sediment sampling

Pore water samples were extracted from all cores at a resolution of 10 cm, using rhizons (Rhizosphere Research Products) (Seeberg-Elverfeldt et al., 2005), collecting a minimum volume of ca. 5 mL over 24 h.

205 The pore water was filtered through 0.2  $\mu\text{m}$  pore size cellulose esters (MCE) membrane syringe filters (Merck MF-Millipore) and aliquoted as follows: 1.5 mL transferred into a plastic screw cap vial without further treatment for anion and cation measurements; 2 mL into a glass vial amended with 50  $\mu\text{L}$  saturated  $\text{HgCl}_2$  solution to inhibit microbial activity and sealed without headspace for alkalinity measurements (Edenborn et al., 1985); and 1.5 mL into a plastic screw cap vial mixed with 200  $\mu\text{L}$   $\text{ZnCl}_2$  (20 % weight  $\times \text{vol}^{-1}$ ) to precipitate dissolved hydrogen sulfide as  $\text{ZnS}$  for subsequent sulfide measurements. All samples were stored at +4  $^\circ\text{C}$  until analysis in the home lab.

210 Immediately after core recovery, the lowermost 20 cm of each sediment core were cut off and subsampled for DNA and RNA extraction. The sediment was pushed out of the liner and the outer 1-2 cm of sediment rims were removed with a sterile spatula. Aliquots of the remaining sediment were transferred into gas-tight aluminum foil bags, flushed with nitrogen gas, heat-sealed and stored at -80  $^\circ\text{C}$  for later extraction of various biomolecules.

hat gelöscht: molecular analyses.

## 2.3 Pore water sulfate, sulfide and alkalinity

Anion concentrations were determined using an Ion Chromatography (IC) System equipped with a SykroGel A  $\times$  300 AB-A01 column (all Sykam). The eluent contained 7.3  $\text{mg} \times \text{L}^{-1}$   $\text{NaSCN}$  and 636  $\text{mg} \times \text{L}^{-1}$   $\text{NaCO}_3$ . The pump rate was set to 1  $\text{mL} \times \text{min}^{-1}$  and the injected sample volume was 50  $\mu\text{L}$ . All samples were measured in triplicates and the results were averaged. Because of their high salt concentrations, all samples had to be diluted 1:50 with MilliQ water before injection. The detection limit of the IC system is 0.5  $\text{mg} \times \text{L}^{-1}$ . The average standard deviation of replicate measurements was always better than 3 %.

225 Sulfide concentrations were measured according to the protocol of Cline (1969). Aliquots with absorption values greater than 1 were diluted and remeasured. Sulfide concentrations were calculated by comparing adsorption values measured for pore water samples to those of a  $\text{Na}_2\text{S}$  standard. The detection limit of the method is 0.1  $\mu\text{M}$ . All samples were measured in triplicates and the results were averaged, with standard deviation  $\leq 3.5$  %.

hat gelöscht: (

hat gelöscht: ,

235 Pore water alkalinity was determined using the Visocolor HE alkalinity AL 7 kit (Macherey-Nagel GmbH).  
As we only had a total of ca. 2 mL of pore water per sample, we scaled down the volume of sample to  
500  $\mu\text{L}$  in order to perform all measurements in triplicates. For this, 10  $\mu\text{L}$  of indicator was added to  
500  $\mu\text{L}$  of pore water and titrated with the Visocolor solution until we observed a change in color from  
blue to orange. Alkalinity of the pore water samples was calculated based on the titration solution volume.  
240 Replicates differed by less than 3 % on average.

#### 2.4 Sulfate reduction rates, modeled sulfate reduction rates

For sulfate reduction measurements, each gravity core was subsampled in triplicate every 40-50 cm and at  
the bottom end. Structurally intact sediment plugs (volume ca. 3.5  $\text{cm}^3$ ) were recovered by inserting 5 mL  
glass barrels fitted with a syringe plunger into the sediment. Following the whole core injection method  
245 (Jørgensen, 1978), 15  $\mu\text{L}$  of radioactive  $^{35}\text{SO}_4$ -sulfate tracer (200 kBq) were injected into the glass barrels  
containing the samples retrieved on the same day (Fossing et al., 2000). The glass barrels were closed  
with butyl rubber stoppers, and the samples incubated at *in situ* temperature (ca. 4  $^\circ\text{C}$ ) for 24 hours. Each  
sample was then transferred into a previously weighed 50 mL centrifuge tube containing 10 mL of 20 %  
zinc acetate solution to stop all microbial activity and to precipitate all volatile hydrogen sulfide as zinc  
250 sulfide. Each vial was then thoroughly shaken to break down all sediment aggregates and stored frozen  
until analysis. Blank samples were prepared by adding the radiolabeled sulfate tracer just before  
transferring the sample into the zinc acetate solution. The tracer blank was prepared in the same way  
without sediment.

Sulfate reduction rates (SRR) were quantified in the home lab, using single-step cold chromium distillation  
255 (Kallmeyer et al., 2004). The sample vials were thawed, centrifuged and the supernatant carefully  
removed. A small aliquot of supernatant was kept for quantification of total radioactivity, the rest was  
discarded. The sediment pellet was then quantitatively transferred into a distillation flask. Due to the  
clayey consistence of the sediments, we had to re-freeze the vials and transfer the frozen sediment pellet  
from the centrifuge tube to the distillation flask. SRR were calculated according to the following formula:

260 Sulfate reduction rate: 
$$\text{SRR} = \frac{\text{SO}_4 \cdot \varphi \cdot a_{\text{tr}} \cdot 1.06 \cdot 10^6}{a_{\text{tot}} \cdot t} \quad (\text{Equation 3})$$

SRR: sulfate reduction rate [ $\text{pmol cm}^{-3} \times \text{day}^{-1}$ ];  $\text{SO}_4$ : sulfate concentration in the pore water [ $\text{mmol} \times \text{L}^{-1}$ ];  
 $\varphi$ : porosity [ $\text{mL} \times \text{cm}^{-3}$ ] of the sediment, set to 0.7;  $a_{\text{tr}}$ : radioactivity of total reduced inorganic sulfur  
[cpm];  $a_{\text{tot}}$ : total radioactivity used in the spiking [cpm];  $t$ : incubation time [d]; 1.06: correction factor for  
isotopic fractionation;  $10^6$ : unit conversion factor from [ $\mu\text{mol} \times \text{L}^{-1}$ ] to [ $\text{pmol} \times \text{L}^{-1}$ ].

265 Assuming steady state conditions, the net rate of sulfate production, or consumption, can be modeled based  
on the measured sulfate concentration profiles by the diffusion-reaction modeling software PROFILE  
(Berg et al., 1998). This software considers three different kinds of vertical transport (i.e. diffusion,  
bioturbation, irrigation) together with the flux across the SWI. The final output corresponds to the  
270 minimum number of intervals, as defined by their respective sulfate production or consumption rates, that  
are necessary to reproduce the measured pore water profiles. For the modeling calculation, we used:  
coefficient of sulfate diffusion in water at 4 °C  $D_{\text{Sulfate}} = 0.56 \times 10^{-5} [\text{cm}^2 \times \text{s}^{-1}]$  (Iversen and Jørgensen  
(1993); porosity  $\varphi = 0.7$ ; and sulfate seawater concentration  $28 \text{ mmol} \times \text{cm}^3$ . Because the sediment  
appeared to be free of macrobenthos, the biodiffusivity and irrigation coefficients were set to  $D_B = 0 \text{ cm}^2$   
 $\times \text{s}^{-1}$ , and  $\alpha = 0$ , respectively.

## 275 **2.5 Methane and carbon dioxide concentrations**

For dissolved  $\text{CH}_4$  and  $\text{CO}_2$  concentrations, we subsampled the lowermost 20 cm of sediment from each  
gravity core directly after recovery. Using 5 mL cut-off syringes, we extracted ca.  $4 \text{ cm}^3$  of sediment per  
core. The first and last  $0.5 \text{ cm}^3$  of sediment in the syringe were discarded while the central  $3 \text{ cm}^3$  were  
transferred into a 10 mL glass crimp vial containing a saturated NaCl solution. The vials were  
280 immediately sealed with thick butyl rubber stoppers, crimped, and stored upside down without headspace  
until analysis in the home lab.

Prior to measurement, we introduced 3 mL of ultrapure helium gas as headspace while withdrawing the same  
amount of NaCl solution from the vial. To equilibrate dissolved gases with the headspace, the content of  
the vials was mixed at 220 rpm on an orbital shaker for 18 h, and further vortexed to break up the  
285 remaining small clayey aggregates. We extracted ca.  $350 \mu\text{L}$  of headspace from the vial using a gas-tight  
syringe. Prior to measurement, ca.  $100 \mu\text{L}$  of the sampled gas were flushed through the injection needle,  
and  $250 \mu\text{L}$  of gas sample were then injected into a 7890A Gas Chromatography System equipped with  
a flame ionization detector (FID), a thermal conductivity detector (TCD) and HP PLOT Q column (all  
Agilent). Oven temperature was set to  $50^\circ\text{C}$ , flow rate to  $17.2 \text{ mL} \times \text{min}^{-1}$  and pressure to 13 psi. The  
290 detectors both worked at  $200^\circ\text{C}$  with flow rates of  $40 \text{ mL} \times \text{min}^{-1}$  (FID) and  $15 \text{ mL} \times \text{min}^{-1}$  (TCD). The  
system was calibrated, using  $250 \mu\text{L}$  of analytic pure standards, injecting  $\text{CO}_2$  concentrations of 310 ppm  
and 5270 ppm, and  $\text{CH}_4$  concentrations of 10 ppm and 5170 ppm. The initial  $\text{CH}_4$  and  $\text{CO}_2$  concentrations  
were converted from ppm to molar concentrations by applying the ideal gas law.



## 2.6 DNA/RNA extractions, sequencing libraries, functional marker genes

295 DNA was extracted for a total of 12 samples from 8 different cores corresponding to 4, 2 and 2 samples from  
HC-affected sites, i.e. Zone 1, Zone 10 and Zone 12, respectively, along with 3 and 1 samples from Ref  
5 and Ref 6, respectively. Samples were subjected to DNA extraction using the DNEasy PowerMax Soil  
Kit (Qiagen, Germany) following manufacturer's instructions with few adaptations. For 2.5 g of starting  
sediment material, the final elution was performed in two steps using twice 2.5 mL of solution C6, and  
300 successively incubated and centrifuged. Eluted DNA was then concentrated by adding 510 µL of a 3M  
sodium acetate (pH 5.2) / glycogen (0.4 µg × µL<sup>-1</sup>) solution and incubated for one hour at -20°C and then  
centrifuged to pellet DNA. After ethanol cleaning and air-drying, DNA was resuspended in 100 µL of 10  
mM Tris buffer. Finally, DNA was cleaned and concentrated using the Zymo DNA Clean & Concentrator  
(Zymo, UK) following the manufacturer's instructions and eluted in a final elution volume of 35 µL.

305 DNA sequencing was achieved by using 32.5 µL of purified and concentrated DNA for metagenomic library  
preparation with the QIAseq FX DNA library UDI A/B kit (Qiagen, Germany) irrespective of the  
individual sample concentrations. The genomic DNA was enzymatically fragmented for 10 min and DNA  
libraries were prepared with 7 PCR cycles for the PCR-less procedure, and without dedicated PCR step  
for the PCR-free procedure. The average library sizes were ±400 base pairs. Prepared libraries were  
310 quantified using a Qubit fluorometer (ThermoFischer, USA) and quality-checked on a Bioanalyzer  
(Agilent, USA). Sequencing was performed on an Illumina NextSeq2000 platform using 2 × 151 bp read  
length at the Luxembourg Centre for Systems Biomedicine (LCSB) Sequencing Platform, aiming at an  
average of 10 Giga base pairs per sequencing library.

RNA was extracted from 2 × 5 g of sediment per sample, using the RNeasy PowerSoil Total RNA kit  
315 (QIAGEN) according to the manufacturer's instructions, yielding 30 µL of RNA-containing extract, and  
quantified on a Qubit4 fluorometer, using the RNA high sensitivity kit (ThermoFisher Scientific). RNA  
extracts were directly subjected to library preparation in technical duplicates, using the Revelo™ RNA-  
Seq High Sensitivity kit (Tecan Life Sciences) with 8 µL of RNA extracts as template. This trio kit  
includes first and second strand cDNA synthesis, adaptor ligation and library amplification through 10  
320 PCR cycles. Prepared libraries were quantified using a Qubit4 fluorometer (ThermoFisher Scientific) and  
quality-checked on a Bioanalyzer (Agilent) to determine the molarity and overall size distribution of RNA  
molecule fragments. The average library fragment size was ± 300 bps and the yields were between 4 and  
12 ng × µL<sup>-1</sup>. Metatranscriptomic libraries displaying high and low molarities were pooled into two

hat gelöscht: positive

hat gelöscht: plus

hat gelöscht: 6

hat gelöscht: as follow

hat gelöscht: two times

hat gelöscht: ml

hat gelöscht: two incubations

hat gelöscht: two centrifugations.

hat gelöscht: 510µl

hat gelöscht: Sodium Acetate

hat gelöscht: Glycogen

hat gelöscht: /

hat gelöscht: 10mM

hat gelöscht: with

hat gelöscht: done

hat gelöscht: using

hat gelöscht: -

hat gelöscht: samples

hat gelöscht: -

hat gelöscht: samples

hat gelöscht: p

hat gelöscht: -

hat gelöscht: instrument

hat gelöscht: (Gbps)

hat gelöscht: 2x5

hat gelöscht: extractss

hat gelöscht: RNA

different batches, and [both](#) sequenced at the EMBL GeneCore (<https://www.embl.org/>) on a NextSeq 2000 with a P3 kit and an Illumina micro kit ( $2 \times 150$  bps), respectively.

hat gelöscht: both

*De novo* assembly of metagenomic reads was performed (Table S1) using a customized Snakemake workflow (Mölder et al., 2021), including quality-control, binning into contigs, gene prediction and annotation as described in [Bornemann et al. \(2023\)](#). Paired-end reads were interleaved, Illumina adapters and controls removed, reads quality-based trimmed, and de-interleaved into forward and reverse read files. Bacterial and archaeal scaffolds were concatenated and mapped back to raw reads to retrieve coverage, % GC and contig lengths. Genes were then predicted by extracting open reading frames (ORFs) from metagenome-assembled scaffolds using Prodigal (Hyatt et al., 2010). Metatranscriptomic reads were quality-filtered and trimmed using Trimmomatic (Bolger et al., 2014). Functional profiles were obtained by mapping the filtered and trimmed reads to their corresponding metagenomic databases using BWA-mem (Li and Durbin, 2009). ORFs were retrieved using Bakta (Schwengers et al., 2021) and combined with the mapping using the featureCounts tool (Liao et al., 2014).

hat gelöscht: (

hat gelöscht: ..

hat gelöscht:

Taxonomic identifications of all ORFs were further integrated with functional annotations by performing [BLASTp](#) searches against an aggregated database of predicted proteins (<https://github.com/williamorsi/MetaProt-database>), using DIAMOND protein aligner v. 0.9.24 (Buchfink et al., 2015). Cut-off values for assigning the best match to specific taxa present in the aggregated database were performed at a minimum bit score of 50, minimum amino acid similarity of 60, and an alignment length of 50 residues. We used this approach to draw conclusions about metabolic traits derived specifically from [-phylum](#) to class taxonomic levels only (Vuillemin et al., 2020a; Vuillemin et al., 2020b).

hat gelöscht: BlastP

Here, we focus on ORFs encoding genes involved in sulfur cycling and methane-related processes only. To trace metabolic potential in anaerobic respiration of sulfur compounds (i.e. sulfate, sulfite, thiosulfate, sulfur, polysulfide), we looked for the presence of ORF- encoding genes with similarity to [adenyllysulfate reductase \(\*apr\*\)](#), dissimilatory sulfite reductase (*dsr*), anaerobic sulfite reductase (*asr*), thiosulfate/polysulfide reductase (*phs/psr*), and sulfhydrogenase (*hyd*) (Vuillemin et al., 2022). For methane production and anaerobic consumption, we targeted ORFs encoding proteins of the methyl coenzyme M reductase (*mcr*). To identify and characterize metabolically active taxa, we targeted the small subunit ribosomal ribonucleic acid (SSU rRNA) as a taxonomic marker and the filamenting temperature-sensitive mutant A-Z (*FtsAZ*) for cell division.

hat gelöscht: phylum

hat gelöscht: ), adenylylsulfate reductase (*apr*)

To confirm taxonomic assignments and metabolic activity of taxa involved in sulfate reduction and AOM processes, we performed a phylogenetic analysis of the RNA polymerase sigma factor (*rpoD*) and ribosomal protein S3 (*rps3*) gene proteins, *aprAB*, *dsrAB*, *mcrA* and *hydB* that we could detect in the transcriptomes (Vuillemin et al., 2020a). All ORFs annotated to these genes were aligned against their top two BLASTp hits in the NCBI database, using MUSCLE (Edgar, 2004). Conserved regions of the alignments were selected using Gblocks 0.91b (Castresana, 2000) with the following settings: allowing for smaller final blocks, gap positions within the final blocks and less strict flanking positions (<http://phylogeny.lirmm.fr/>). Phylogenetic analysis of the resulting amino acid alignments of the predicted proteins were conducted in SeaView version 5.0.5 (Gouy et al., 2010), using PhyLM maximum likelihood (Guindon et al., 2010), with BLOSUM62 as the evolutionary model and 100 bootstrap replicates.

hat gelöscht: R

hat gelöscht: *dsrA-G*,

hat gelöscht: and

hat gelöscht: -G

hat gelöscht: (Supplementary Fig. S4-7).

### 3. Results

#### 3.1 Pore water geochemical profiles

All sulfate concentrations in the uppermost profiles roughly match the sulfate concentration of the Barents Sea bottom waters (ca. 28 mM). In all cores, sulfate concentrations decrease almost linearly with depth, linear regressions showing correlation coefficients of  $R^2 > 0.85$  (Fig. 2a-2b and Supplementary Fig. S1). The slopes of the regression lines can be divided into two groups corresponding to one group encompassing reference sites Ref 5 and Ref 6, and another group including the three HC-affected sites Zone 1, Zone 10 and Zone 12. Based on a t-test using the software PAST v. 3.20 (Hammer et al., 2001), the slopes of these two groups are statistically significantly different ( $t = 5.574$ ,  $p = 1.25E-6$ ) from each other (Fig 2). The sulfate profiles from HC-affected sites show a steeper decrease with depth than those from reference sites. On average, sulfate concentrations decrease by  $10 \text{ mmol} \times \text{m}^{-1}$ , which would correspond to complete sulfate depletion at roughly 3 mbsf at HC-affected sites. At reference sites, the average slope is  $3 \text{ mmol} \times \text{m}^{-1}$  with little variations, which implies that sulfate would be depleted at ca. 12 mbsf.

hat gelöscht: 2

hat gelöscht: , with

hat gelöscht: zones

hat gelöscht: the other

hat gelöscht: positive

hat gelöscht: Those

hat gelöscht: not significant

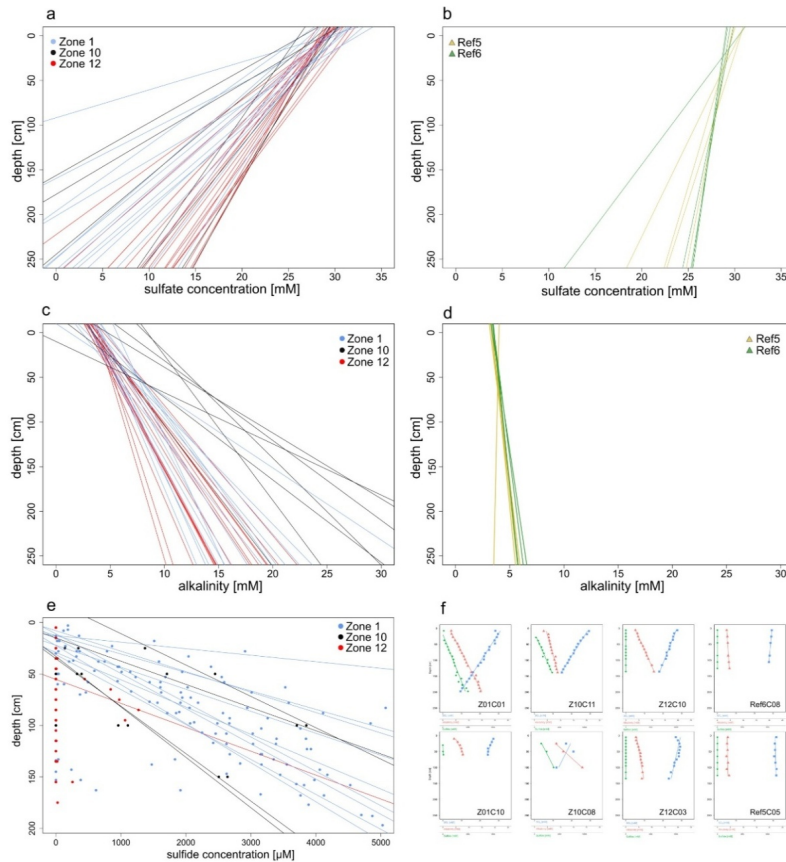
hat gelöscht: , but the trend is clearly visible

hat gelöscht: positive

hat gelöscht: m below seafloor (

hat gelöscht: )

hat gelöscht: positive



430

**Figure 2. Pore water profiles for sulfate concentrations, alkalinity, sulfite, and subset of representative profiles. (a, b) Regression lines for sulfate profiles are all linear ( $R^2 > 0.85$ ) and show decreasing trends with depth. The regression lines calculated for (a) HC<sub>2</sub>-affected sites (Zone 1, Zone 10, Zone 12) show a steeper slope than those calculated for (b) reference sites (Ref 5, Ref 6). (c, d) Regression lines of pore water alkalinity are linear ( $R^2 \geq 0.85$ ) and increase with depth. The regression lines calculated for (c) HC<sub>2</sub>-affected sites show a less steep gradient than (d) those of reference sites. (e) Sulfide concentrations**

435

hat gelöscht: all

hat gelöscht: pore water concentration profiles. All

hat gelöscht: a

hat gelöscht: trend

hat gelöscht: the

hat gelöscht: positive

measured for all cores from HC-affected sites (dots) with their corresponding regression lines when sulfide concentrations were quantifiable. (f) Subset of representative profiles selected for each sampling site. The uppermost and lowermost rows depict the core exhibiting the highest and lowest regression coefficient (i.e.  $R^2$  value) across HC-affected and reference sites, respectively.

445

All alkalinity profiles display a clear linear increase with depth ( $R^2 \geq 0.85$ ). From  $5 \text{ mmol} \times \text{L}^{-1}$  at the SWI, pore water alkalinity increases differently with depth, corresponding to 8, 5 and  $6 \text{ mmol} \times \text{L}^{-1} \times \text{m}^{-1}$  at HC-affected sites Zone 1, Zone 10, and Zone 12, and  $\leq 1 \text{ mmol} \times \text{L}^{-1} \times \text{m}^{-1}$  at reference sites Ref 5 and Ref 6, respectively (Fig. 2c-2d and Supplementary Fig. S2).

450

Based on the slopes of pore water profiles, the calculated alkalinity fluxes are larger at HC-affected sites than at reference sites. The same is true for sulfate fluxes, but differences across HC-affected sites and reference sites are less pronounced (Supplementary Fig. S3). In comparison, variations observed within each sampling site are small.

455

Sulfide could hardly be detected in pore water samples collected from reference sites, most values being below  $1 \mu\text{M}$ . In contrast, sulfide was detected in most of the cores from HC-affected sites. Especially at Zone 1 and Zone 10, sulfide concentrations increase linearly with depth (Fig. 2e). The majority (ca. 70 %) of the cores from Zone 1 show an increase of  $2.5 \text{ mM} \times \text{m}^{-1}$  in sulfide concentrations. One core (Z01C03) stands out, reaching sulfide concentrations of ca. 11 mM at 1 mbsf. Several cores (ca. 57 %) from Zone 10 show a binary distribution of sulfide concentrations, corresponding either to linear profiles reaching ca. 1mM sulfide at 1 mbsf, or to a steeper increase reaching ca. 3.7 mM at the same depth. At Zone 12, sulfide is detectable in only 2 of the 17 cores, with much lesser increase in concentrations compared to Zone 1 and Zone 10.

460

### 465 3.2 Measured and modeled sulfate reduction rates

SRR were detectable in only 29 out of the 50 cores (Fig. 3), with rates between 4 and  $320 \text{ pmol} \times \text{cm}^{-3} \times \text{d}^{-1}$ . In 403 of the 455 samples across the 50 cores analyzed (i.e. 89 %), SRR were below the detection limit ( $1 \text{ pmol} \times \text{cm}^{-1} \times \text{d}^{-1}$ ). The occurrence of very low but detectable SRR increased with sediment depth, which mostly stands true for HC-affected sites (Fig. 3).

hat gelöscht: positive

hat gelöscht: 3

hat gelöscht: positive

hat gelöscht: (Fig. S3).

hat gelöscht: applies to

hat gelöscht: positive

hat gelöscht: positive

hat gelöscht: 4

hat gelöscht: that increase much less

hat gelöscht:

hat gelöscht: 5

hat gelöscht: positive

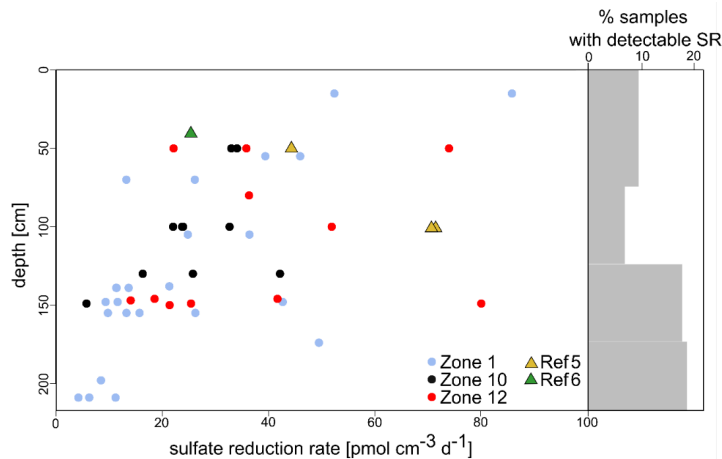


**Figure 3. Sulfate reduction rates (SRR) and percentages of samples with sulfate reduction rates above the detection limit.** Low SRR became increasingly detectable with increasing sediment depth. The number of samples with measurable SRR (% grey bars) is higher in sediments from HC-affected sites (dots) compared to reference sites (triangles), *n.B.* due to a lack of samples, the two uppermost intervals were merged.

485 Diffusion-reaction modeling with PROFILE (Berg et al., 1998) suggests steady SRR in 47 of the 50 cores (Supplementary Fig. S1), implying that SRRs remain constant over the entire length of the cores. The modeled SRR profiles show SR activity (i.e.  $>0 \text{ pmol} \times \text{cm}^{-3} \times \text{d}^{-1}$ ) in 33 cores, of which 6 display rates  $\leq 0.01 \text{ pmol} \times \text{cm}^{-3} \times \text{d}^{-1}$ , and 27 with supposed SRR  $\geq 1 \text{ pmol} \times \text{cm}^{-3} \times \text{d}^{-1}$ . For three specific cores (i.e. Z01C02, Z01C09, Z12C17), PROFILE proposes two intervals with different SRRs, suggesting that SR processes may only be active in the upper 50 cmbsf and inactive in the sediment below.

495 The modeled and measured SRR are indicative of net and gross turnover rates, respectively. The gross rate reflects microbial turnover whereas the net turnover rate includes the recycling of reduced sulfur compounds (Berg et al., 1998). The modeled (i.e. net) rates for most samples are higher than the measured (i.e. gross) rates, which is rather unusual and can be explained by very low values whose absolute changes have a drastic effect on the calculated values. The modeled and measured SRR are nevertheless within the same order of magnitude, and thus comparable.

500

### 3.3 Methane and carbon dioxide concentrations

All samples contain measurable methane concentrations, ranging from 0.08 to 19.79  $\mu\text{mol} \times \text{L}^{-1}$ . All samples from reference sites contain less than 5  $\mu\text{mol} \times \text{L}^{-1}$  of methane, detection of any higher concentrations being restricted to some samples from HC-affected sites and only below 100 cmbsf (Fig. 4). CO<sub>2</sub> was detectable in all samples, with concentrations ranging from 29  $\mu\text{mol} \times \text{L}^{-1}$  to 512  $\mu\text{mol} \times \text{L}^{-1}$ , but without any specific trend with depth (Fig. 4). The reason is probably that any CO<sub>2</sub> from whichever source enters the carbonate equilibrium and the gas is removed from the pore water, both in HC-affected sites and reference sites. The low methane and carbon dioxide concentrations prevented any measurement of their stable isotopic signatures.

hat gelöscht: only in

hat gelöscht: positive

hat gelöscht: cm sediment depth

hat gelöscht: 6) we were able to detect any higher concentrations....

hat gelöscht: 6). Such

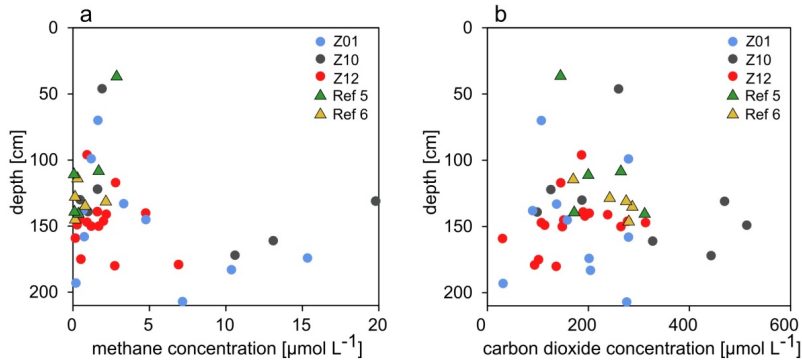


**Figure 4. Concentrations of dissolved methane and carbon dioxide. (a)** At HC-affected sites, methane concentrations are highest in samples originating from 100 cmblf or deeper, whereas methane concentrations at reference sites remain below 5  $\mu\text{mol} \times \text{L}^{-1}$ . **(b)** CO<sub>2</sub> concentrations across samples do not display any specific trend with sediment depth.

### 3.4 Statistical correlations

To identify geochemical differences between HC-affected and reference sites, we performed a Pearson correlation analysis. Correlation coefficients calculated for each separate gravity core (Table S2) indicate that alkalinity is strongly negatively correlated ( $p \geq -0.85$ ) with sulfate concentrations in sediments from HC-affected sites. The same applies to quantifiable sulfate and sulfide concentrations ( $p \geq -0.7$ ). For

hat gelöscht: positive

hat gelöscht: positive

reference sites, alkalinity and sulfate concentrations are also strongly correlated ( $p \approx 0.8$ ), whereas sulfide concentrations are below the detection limit and hence have been omitted for the correlation analysis.

530 We established ratios of sulfate to alkalinity ( $\text{HCO}_3^-$ ) fluxes (Fig. 5). As about 90% of seawater alkalinity can be contributed to carbonate ( $89.8\% \text{HCO}_3^-$ ,  $2.9\% \text{CO}_3^{2-}$ ) (Kerr et al., 2021) we set alkalinity synonymous with carbonate concentration. We compared the measured fluxes to those expected from organoclastic (1:2 based on Eq. 1) and methanotrophic (1:1 based on Eq. 2) SRR activities. At reference sites, the average ratio of sulfate to alkalinity fluxes equals 2:1 whereas it is 1.25:1 (5:4) at HC-affected sites, imply  
 535 that either  $\text{HCO}_3^-$  is being removed from the pore water, or that pore water sulfate is eventually being replenished via sulfide oxidation.

hat gelöscht: and compared them

hat gelöscht: positive

hat gelöscht: ,

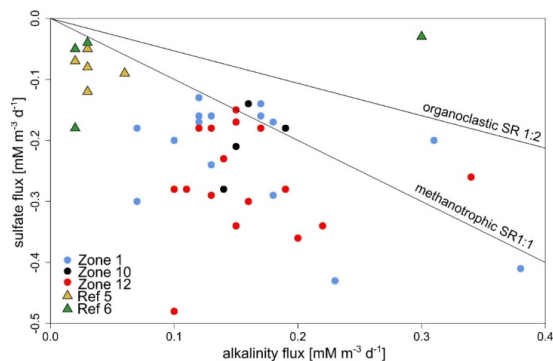


**Figure 5. Relationship between sulfate and alkalinity fluxes at HC-affected sites and reference sites.**

540 The majority of samples from HC-affected sites (dots) have lower alkalinity than sulfate fluxes. This is even more pronounced at reference sites (triangles). Black lines signify theoretical ratios for methanotrophic (1:1) and organoclastic (1:2) SR.

### 3.5 Functional marker genes specific to the SMTZ

545 From the 12 sequenced metagenomes, we extracted a total of 307 234 ORFs with multiple annotations that corresponded to 821 850 predicted genes. From the 5 sequenced metatranscriptomes, we extracted a total of 31 093 ORFs corresponding to 47 316 predicted genes (Supplementary Table S2).



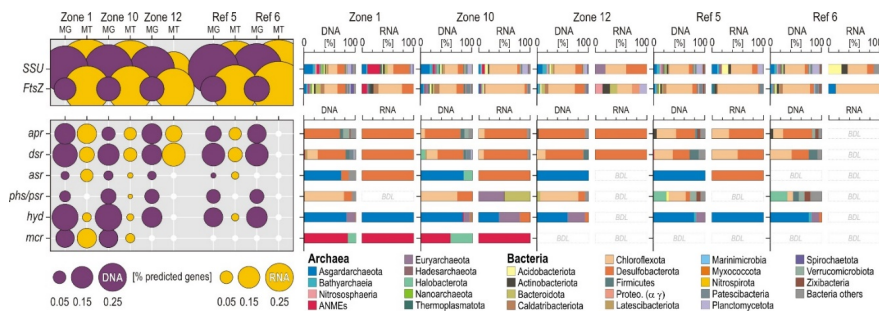


**Figure 6. Open reading frames encoding functional marker genes involved in sulfate reduction, production and anaerobic consumption of methane and their taxonomic assignments at the phylum to class level.**

The relative abundances of certain phyla increase at HC-affected sites compared to reference sites. Concomitant expression of *apr* and *dsr* genes by Desulfobacterota, *phs* genes by Chloroflexota, *hyd* genes by Asgardarchaeota, and *mcr* genes by ANMEs and Halobacterota are consistent with methanotrophic sulfate-reducing activities. **Abbreviations** - *apr*: adenylylsulfate reductase; *dsr*: dissimilatory sulfite reductase; *asr*: anaerobic sulfite reductase; *phs/psr*: thiosulfate and polysulfide reductase; *hyd*: sulphydrogenase; *mcr*: methyl coenzyme M reductase; MG: Metagenomics; MT: Metatranscriptomics; BDL: below detection limit.

For each of the targeted marker genes, we plotted the relative percentage of total predicted genes and their corresponding taxonomic assignments at the phylum and class level (Fig. 6). Taxonomic assignments of SSU rRNA and *FtsAZ* proteins show that metabolically active and growing microbial populations at HC-affected sites are affiliated with the phyla Chloroflexota, Desulfobacterota and Euryarchaeota, and more specifically with anaerobic methanotrophs (i.e. ANMEs). The phyla Desulfobacterota and Chloroflexota are actively engaged in processes of sulfate reduction, as shown by the expression of ORFs encoding the *aprAB* and *dsrAB* genes (Fig. 7a-7b). Taxonomic assignments of expressed ORFs encoding *mcrA* genes show an increased abundance of methanotrophic ANMEs (Fig. 7c) over methanogenic Halobacterota. ORFs encoding *hydB-G* genes are expressed by taxa related to the class Lokiarchaeia and Thorarchaeia (Fig. 7d) among the phylum Asgardarchaeota, indicating metabolic capability to use reduced sulfur compounds (e.g. polysulfide, elemental sulfur). However, their overall expression levels appear limited and these Asgardarchaeota do not seem to actively divide (Fig. 6). At reference sites, Chloroflexota appear to be the only phylum capable of growing and dividing in these organic-poor sediments (Fig. 6). However,

**hat gelöscht:** The relative abundances of certain phyla increase at HC-affected sites. Concomitant expression of *dsr* and *apr* genes by Desulfobacterota, *phs* genes by Chloroflexota, *hyd* genes by Asgardarchaeota, and *mcr* genes by ANMEs and Halobacterota are consistent with methanotrophic sulfate-reducing activities. **Abbreviations** - *dsr*: dissimilatory sulfite reductase; *apr*: adenylylsulfate reductase; *asr*: anaerobic sulfite reductase; *phs/psr*: thiosulfate and polysulfide reductase; *hyd*: sulphydrogenase; *mcr*: methyl-coenzyme M; MG: Metagenomics; MT: Metatranscriptomics; BDL: below detection limit.

**hat gelöscht:** 4

**hat gelöscht:** 8

**hat gelöscht:** positive

**hat gelöscht:** *dsr*

**hat gelöscht:** *apr*

**hat gelöscht:** 8).

**hat gelöscht:** . Taxonomic assignments of expressed ORFs encoding *mcr* genes show an increased abundance of methanotrophic ANMEs over methanogenic Halobacterota.

concomitant expression of functional marker genes involved in sulfate reduction remains below the limit of detection. We acknowledge that the non-detection of certain genes may also result from limited sequencing depths.

595

Phylogenetic trees plotted for transcript ORFs assigned to the *rps3* and *rpoD* taxonomic marker genes (Supplementary Figs. S4-S5) provided concomitant evidence for metabolic activity by the phyla Desulfobacterota, Chloroflexota (class Dehalococcoidia), Acidobacterota (class Aminicenentia), Asgardarchaeota (class Thorarchaeia), and Halobacterota (class ANME-1).

600



**Figure 7. Phylogenetic trees of *aprAB*, *dsrAB*, *mcrA* and *hydB-G* protein-encoding genes.** PhyML maximum likelihood trees of transcript ORFs encoding: **(a)** the adenylylsulfate reductase (714 amino acids) subunit alpha (*aprA*) and beta (*aprB*); **(b)** the dissimilatory sulfite reductase (493 amino acids) subunit alpha (*dsrA*) and beta (*dsrB*); **(c)** the methyl coenzyme M reductase reductase (698 amino acids) subunit alpha

605

(*mcrA*); and (d) the sulfhydrogenase, or sulfur reductase (286 amino acids), subunit beta (*hydB*) and gamma (*hydG*). Phylogenetic trees are based on 100 bootstrap replicates with BLOSUM62 as evolutive model. Boldface types signify sequence accession numbers to the NCBI database.

#### 4. Discussion

##### 610 4.1 Pore water geochemical profiles correlate to meta-omics features

Pore water profiles reflect the spatial distribution of net turnover processes. The shape of the profile allows to distinguish intervals in which transport is purely diffusive (i.e. linear profile) from those in which there is either net production (i.e. convex profile) or consumption (i.e. concave profile) of chemical species (Schulz, 2006; Hesse and Schacht, 2011).

615 Based on the largely linear profiles for pore water alkalinity, sulfate and sulfide (Figs. 2-3, Figs. S1-S2), we infer the absence or near-absence of net sulfate consumption in the depth interval covered by the cores, and a sink for sulfate as well as a source of sulfide and alkalinity at greater depth. Microbially-mediated AOM with sulfate as electron acceptor yields hydrogen sulfide, bicarbonate and water (Eq. 2), providing an explanation for both sink and source (Martens and Berner, 1974; Iversen and Jorgensen, 1985), assuming sufficient supply of methane at greater depth. The occurrence of AOM at deeper depth is further supported by the relationship between sulfate and alkalinity fluxes (Fig. 5) and negligibly small methane concentrations ( $< 10 \mu\text{M L}^{-1}$ ) at the bottom end of all cores from HC-affected sites and reference sites (Fig. 4), indicating almost complete consumption of methane originating from biogenic or thermogenic sources below our sampling interval.

625 Linear concentration profiles are only obtained in regions with no net consumption or production of the respective compound (Schulz, 2006). Despite the apparent linearity of sulfate profiles (Fig. 2), we observed very low SRR ( $\leq 300 \text{ pmol} \times \text{cm}^{-3} \times \text{d}^{-1}$ ), confirming previous reports of sporadic SRR in Barents Sea sediments with similar rates above the SMTZ (Nickel et al., 2012). In our case, sulfate reduction is mainly detectable at HC-affected sites (Fig. 3), with a greater prevalence in deeper sediments (Fig. 5). With seepage supplying electron donors, like methane and/or other HCs, from deeper reservoirs to near-surface sediment, sulfate reduction is fuelled by those HCs rather than from the buried and more recalcitrant OM. Inconspicuous supplies of methane and/or other HCs to the overlying sediment can stimulate SRR by providing alternative electron donors. Such sporadic energy supply promotes geochemical conditions that stimulate benthic HC-degrading microbial communities. Although these

hat gelöscht: 7

hat gelöscht: gas

hat gelöscht: positive

hat gelöscht: (Schulz, 2006).

hat gelöscht: ,

hat gelöscht: positive

hat gelöscht: ,

hat gelöscht: higher occurrence

hat gelöscht: organic matter.

hat gelöscht: above

645 communities can be physiologically and phylogenetically diverse, they are mainly composed of anaerobic guilds of methanogens, methanotrophs, sulfate reducers and fermenters (Teske, 2019).

The analysis of functional marker genes supports the notion of sporadic HC supply, providing complementary insights into the metabolic potential and activity of specific microbial populations in the sediment. The occurrence and abundance of *aprAB*, *dsrAB*, and *mcrA* genes supports interpretations of geochemical data in terms of sulfate-driven AOM processes and metabolic activity (Fig. 6). Taxonomic profiling of populations expressing ORFs encoding genes involved in sulfate reduction (i.e. *aprAB*, *dsrAB*) reveals Desulfobacterota (family Desulfobacteraceae) and Chloroflexota (class Dehalococcoidia) as the prevalent bacterial phyla constituting the consortium of sulfate-reducing bacteria at HC-affected sites (Fig. 7, Supplementary Figs. S4-S5). The *aprAB* and *dsrAB* phylogenetic trees clearly show that none of these genes correspond to their reverse function and the ORFs annotated as *aprAB* and *dsrAB* are predicted to function in dissimilatory sulfate reduction. Moreover, the sediment being fully anoxic, any detection of sulfur oxidation via reversible *aprAB* or reverse *dsrAB* was unexpected as such activities are mostly reported for aerobic Gammaproteobacteria (Vuillemin et al., 2022).

660 Further, ORFs encoding genes involved in anaerobic production and consumption of methane (i.e. *mcrA*) clearly show that the clade ANME-1 exhibits concomitant, although low metabolic activity towards anaerobic oxidation of methane (Fig. 7c), namely they express ORFs encoding the reversible *mcrA* gene. The higher expression levels of methanotrophic clade ANME-1 over methanogenic Halobacterota (Fig. 6) also suggest that metabolic activity by ANMEs could be sustained by an alternative source of methane (Dong et al., 2020), although cryptic production of biogenic methane by the ANME-1 clade has also been observed in experiments replicating SMTZ conditions (Beulig et al., 2019). Because methane concentrations measured at both HC-affected sites and reference sites were similarly low (Fig. 4), it appears unlikely that AOM processes are sustained by in situ production of biogenic methane only (Dong et al., 2020). Finally, the class Lokiarchaeia and Thorarchaeia in the phylum Asgardarchaeota expressed ORFs encoding beta and gamma subunits of *hydB-G* genes (Fig. 7d), and thereby appear metabolically active, using various sulfur and sulfide species, potentially produced as by-products of sulfate reduction.

670 In contrast, Chloroflexota (class Dehalococcoidia) was the only phylum at reference sites showing sufficient metabolic activity was adequate to achieve cell division (i.e. *FstAZ*). In the absence of an univocal signal towards active dissimilatory sulfate reduction by Dehalococcoidia at HC-affected sites (Fig. 7b), we infer that these Chloroflexota could persist and gain energy through fermentation processes in organic-lean marine sediments instead (Vuillemin et al., 2020a). Due to this metabolic versatility, Chloroflexota were

hat gelöscht: ¶

hat gelöscht: *aprAB*,

hat formatiert: Schriftart: Nicht Kursiv

hat formatiert: Schriftart: Nicht Kursiv

hat gelöscht: *aprAB*

hat formatiert: Schriftart: Nicht Kursiv

hat formatiert: Schriftart: Nicht Kursiv

hat gelöscht: positive

hat gelöscht: 8

hat gelöscht: -S6).

hat gelöscht:

hat formatiert: Schriftart: Nicht Kursiv

hat gelöscht:

hat gelöscht: 8, Supplementary Fig. S7

hat formatiert: Schriftart: Nicht Kursiv

hat gelöscht: positive

hat gelöscht: ,

hat formatiert: Schriftart: Nicht Kursiv

hat gelöscht: the

hat gelöscht: ,

hat gelöscht: appears

hat formatiert: Schriftart: Nicht Kursiv

hat gelöscht: through

hat gelöscht: where its

hat gelöscht: a clear

hat formatiert: Schriftart: Nicht Kursiv

hat gelöscht: sulfur turnover processes (Supplementary

hat gelöscht: S5

695 [found to be active at both HC-affected and reference sites, which rank them as poor microbial indicators for inconspicuous HC seepage \(Iasakov et al., 2022\).](#)

Together, these microbial patterns extracted from meta-omics corroborate the geochemical data, arguing in favor of [discrete](#) AOM processes concomitant to sulfate reduction at [HC-affected sites](#), and for limited in situ production of biogenic methane at both [HC-affected sites](#) and reference sites. [Alongside an active AOM consortium composed of Desulfobacterota and ANME-1, concomitant](#) production of reduced sulfur compounds could apparently stimulate metabolic activity by [Lokiarchaeia and Thorarchaeia \(Figs. 6 and 7\).](#)

#### 4.2 Geochemical indicators for inconspicuous HC seepage

705 [The combined use of meta-omics microbial patterns, with the determination of SR and related geochemical features and fluxes in upper sediments, enables to a certain extent](#) to distinguish between [HC-affected](#) sites and reference sites. Sediments of the SW Barents Sea are organic-poor (TOC <0.5 %), and thus characterized by a lack of electron donors (Knies and Martinez, 2009) and low microbial activity (Nickel et al., 2012; Nickel et al., 2013) with consequent sulfate penetration to greater sediment depths. In organic-rich sediments, any signal inherent to minor HC seepage fueling SR would be difficult to detect as it would be covered by organoclastic SR processes. The organic-lean nature of Barents Sea sediments should enable the detection of discrete HC seeps, because the slightest supply of electron donors leads to a direct increase in the metabolic activity of HC-degrading microbial populations. This slight increase in metabolic activity can then be discriminated from the background signal observed at reference sites. Diffusion of HCs was thus expected to promote sulfate consumption, resulting in its depletion in the pore water at shallower sediment depths. This, combined with variable fluxes of thermogenic and biogenic methane, can account for variations in the depth of the SMTZ.

715 At different locations of the SW Barents Sea, the depth of the SMTZ, or rather the sulfate depletion depth, was postulated, for instance, at 37 mbsf in the Hammerfest/Loppa High and the Tromsø Basin/Ingøydjupet area (Nickel et al., 2012), and between 3.5 and 29.2 mbsf in the Ingøydjupet area (Argentino et al., 2021a). These values are consistent with the global average [depth of the SMTZ](#) ( $12.8 \pm 12.1$  mbsf) on the continental slope (Egger et al., 2018). For comparison, at the Vestnesa Ridge which is under the influence of gas hydrates, the depth of the SMTZ fluctuates massively between seepage (ca. 1 mbsf) and non-seepage (ca. 3 to 75 mbsf) sites (Hong et al., 2016). Similarly, [Barents Sea sediments with](#)

**hat gelöscht:** positive

**hat formatiert:** Schriftart: Nicht Kursiv

**hat gelöscht:** positive

**hat gelöscht:** The

**hat gelöscht:** Asgardarchaeota. Due to their metabolic versatility, Chloroflexota were found to be active at both HC positive and reference sites, which rank them as poor microbial indicators for inconspicuous HC seepage (Iasakov et al., 2022).

**hat gelöscht:** In addition to the

**hat gelöscht:** extracted from meta-omics that allow

**hat gelöscht:** positive

**hat gelöscht:** , and the occurrence of sulfate reduction in the upper sediment, some geochemical features are also useful to distinguish HC and reference sites in the Barents Sea

**hat gelöscht:** SMTZ

**hat gelöscht:** in the B

740 and without methane seeps show an SMTZ located between a few cm and about 2 mbsf (Argentino et al., 2021b).

Linear extrapolation of sulfate profiles (Fig. 2) indicates complete sulfate depletion, indicative of an SMTZ, at 12 and 3 mbsf for reference and HC-affected sites, respectively. We suggest that the difference in sulfate penetration depth is caused by upwards migration of HCs. The sulfate and alkalinity fluxes inherent to organoclastic (Eq. 1) and methanotrophic (Eq. 2) SR have respective theoretical ratios of 1:2 and 1:1, while mixed SR processes have intermediate values. Current ratios of sulfate to alkalinity fluxes (Fig. 5) at reference sites imply that either HCO<sub>3</sub><sup>-</sup> is being removed from the pore water, or that pore water sulfate is eventually being replenished via sulfide oxidation. From previous work in the area, we know that the sediment is fully anoxic below the uppermost few cm. Phylogenetic analysis of *aprAB* and *dsrAB* genes clearly shows that none of the identified amino acid sequences correspond to their reverse function. Further, we did not identify any *dsrC* sequences, which potentially work in cellular sulfur oxidation (Ruiz-Blas et al., 2024). While dissolved inorganic carbon (DIC) can be assimilated via acetogenesis, methanogenesis, or methanotrophy (Kellermann et al., 2012), authigenic carbonate minerals are known to precipitate from the pore water as by-products of AOM processes (Turchyn et al., 2021), sometimes even forming carbonate hardground at the seabed. However, from the low level of detection of AOM-related transcripts, we inferred only a minor imprint on the geochemistry, suggests is, and therefore assume that carbonate ions originating from AOM processes at greater depths are diffusing upward and eventually precipitate as calcium carbonate. Up to 80 % of the sulfide produced through SR can also be converted back into sulfate through reoxidation of reduced sulfur compounds (Jørgensen et al., 2004) and disproportionation (Pellerin et al., 2015; Jørgensen et al., 2019a). Finally, the dissolution of sulfate minerals, such as barite (BaSO<sub>4</sub>), may also act as an additional source of sulfate (Griffith and Paytan, 2012). Altogether, this suggests either the reoxidation of sulfide, or the removal of bicarbonate from the pore water, e.g. by mineral precipitation, or both. The former is further supported by concomitant sulfate reduction, detected by radiotracer incubations (Fig. 3) and microbial gene expression patterns (Fig. 6), the latter by the ratios of sulfate to alkalinity flux (Fig. 5). Thus, we could identify several biogeochemical features that argue for ongoing sulfate reduction (most likely AOM-related) at HC-affected sites below our sampled depth range, which allow their discrimination from reference sites. Given the sulfate concentration profiles and the scarce methane data, it becomes clear that AOM is not a quantitatively important process in the cored depth interval, producing an erratic signal in HC-affected sediments.

hat gelöscht: centimeters depth

hat gelöscht: 5

hat gelöscht: the

hat gelöscht: positive

hat gelöscht: ing

hat gelöscht: ¶

hat gelöscht: , respectively,

hat gelöscht: i.e. 2:1 at HC positive sites,

hat gelöscht: :4 (i.e. 1.25:1

hat gelöscht: )

hat gelöscht: .

hat gelöscht: ¶

hat gelöscht: ,

hat gelöscht: .

hat gelöscht: )

hat gelöscht: positive

hat gelöscht: .

## 5. Conclusions

Our study, combining modeled and measured SRR as well as pore water geochemistry with functional marker genes, [revealed](#) remarkable differences between samples originating from a pristine seafloor and those from areas affected by small and inconspicuous HC seepage. The linear shape of pore water profiles was indicative of purely diffusive transport under steady-state conditions and allowed estimation of the depth of sulfate depletion, which [appeared](#) markedly different between HC-affected and reference sites. At the HC-affected sites, we found higher pore water fluxes of sulfate, sulfide and alkalinity, and could also demonstrate active microbial SR by turnover measurements and modeling. Furthermore, meta-omics provided additional evidence for enhanced metabolic activity [related to](#) microbial sulfate reduction coupled [with minor](#) AOM processes at HC-affected sites, which could be clearly discriminated from the background signal inherent to fermentative activities and [minor in situ](#) production of methane by the subseafloor biosphere. These observations demonstrate that [inconspicuous](#) HC seepage, which is not even visible at the seafloor, significantly influences sedimentary biogeochemical cycles driven by microbial populations resident in [organic-lean](#) sediments.

hat gelöscht: meta-omics of

hat gelöscht: showed

hat gelöscht: is

hat gelöscht: positive

hat gelöscht: positive

hat gelöscht: of

hat gelöscht: to

hat gelöscht: positive

hat gelöscht: quasi-absence of

hat gelöscht: methane

hat gelöscht: minor

hat gelöscht: these

hat gelöscht:

## 6. Data availability

Geochemical data, ORFs sequences and their BlastP outputs are available as Supplementary Information.

## 7. Author contributions

JK and RDP organized the sampling cruise. ES and JK designed the study and sampled the cores. ES performed sulfate, alkalinity, SRR and gas analyses. AV, BK, CL and AS performed DNA and RNA analyses. ES and AV wrote the manuscript and all authors contributed to writing and revision.

## 8. Competing interests

The authors declare that they have no conflict of interest.



## 9. Acknowledgments

We thank all crew members of the *SV Sverdrup*, as well as Steffen Okolski, Jan Axel Kitte and Edgar Kutschera for their great help during the sampling cruise. The help of Steffen Okolski during ion chromatography, alkalinity and sulfide measurement procedures and Simone Bernsee during radioisotope experiments is acknowledged.

## 10. Financial support

This research has received funding from the European Union's Horizon 2020 research and innovation programme under grant agreement no. 899667.

### *PROSPECTOMICS Consortium*

The principal investigators of the PROSPECTOMICS project are Jens Kallmeyer<sup>1</sup>, Paul Wilmes<sup>2</sup>, Alexander J. Probst<sup>3</sup>, Dörte Becher<sup>4</sup>, Thomas Ratte<sup>5</sup>, and Rolando di Primio<sup>6</sup>. The project managers are Aurèle Vuillemin<sup>1</sup>, Cédric C. Laczny<sup>2</sup>, André R. Soares<sup>3</sup>, and Anke Trautwein-Schult<sup>4</sup>. Scientists and technicians include Ellen Schnabel<sup>1</sup>, Kai Mangelsdorf<sup>7</sup>, Steffen Okolski<sup>1</sup>, J. Axel Kitte<sup>1</sup>, Benoit J. Kunath<sup>2</sup>, Oskar Hickl<sup>2</sup>, Tuesday Lowndes<sup>2</sup>, Zainab Zafar<sup>2</sup>, Sarah Esser<sup>3</sup>, Anne Ostrzinski<sup>4</sup>, Sebastian Grund<sup>4</sup>, and Alexander Pfundner<sup>5</sup>.

<sup>1</sup>GFZ German Research Centre for Geosciences, Section Geomicrobiology, Telegrafenberg, 14473 Potsdam, Germany; <sup>2</sup>Luxembourg Centre for Systems Biomedicine, University of Luxembourg, Esch-sur-Alzette; <sup>3</sup>Environmental Metagenomics, Research Center One Health Ruhr of the University Alliance Ruhr, Faculty of Chemistry, University of Duisburg-Essen, Essen, Germany; <sup>4</sup>Department of Microbial Proteomics, University of Greifswald, Greifswald, Germany; <sup>5</sup>Computational Systems Biology, Centre for Microbiology and Environmental Systems Science, University of Vienna, Vienna, Austria; <sup>6</sup>Aker BP ASA, Sandvika, Viken, Norway; <sup>7</sup>GFZ German Research Centre for Geosciences, Section Organic Geochemistry, Telegrafenberg, 14473 Potsdam, Germany.

## 11. References

Abrams, M. A.: Marine seepage variability and its impact on evaluating the surface migrated hydrocarbon seep signal, *Marine and Petroleum Geology*, 121, 10.1016/j.marpetgeo.2020.104600, 2020.

- 850 Argentino, C., Waghorn, K. A., Bünz, S., and Panieri, G.: Sulfate reduction and anaerobic oxidation of methane in sediments of the South-Western Barents Sea, *Biogeoscience*, 10.5194/bg-2021-58, 2021a.
- Argentino, C., Waghorn, K. A., Vadakkepuliambatta, S., Polteau, S., Bunz, S., and Panieri, G.: Dynamic and history of methane seepage in the SW Barents Sea: new insights from Leirdjupet Fault Complex, *Sci Rep*, 11, 4373, 10.1038/s41598-021-83542-0, 2021b.
- Berg, P., Risgaard-Petersen, N., and Rysgaard, S.: Interpretation of measured concentration profiles in sediment pore water, *Limnol Oceanogr*, 43, 1500-1510, 10.4319/lo.1998.43.7.1500, 1998.
- 855 Beulig, F., Roy, H., McGlynn, S. E., and Jorgensen, B. B.: Cryptic CH<sub>4</sub> cycling in the sulfate-methane transition of marine sediments apparently mediated by ANME-1 archaea, *ISME J*, 13, 250-262, 10.1038/s41396-018-0273-z, 2019.
- Bolger, A. M., Lohse, M., and Usadel, B.: Trimmomatic: a flexible trimmer for Illumina sequence data, *Bioinformatics*, 30, 2114-2120, 10.1093/bioinformatics/btu170, 2014.
- 860 Bornemann, T. L. V., Esser, S. P., Stach, T. L., Burg, T., and Probst, A. J.: uBin: A manual refining tool for genomes from metagenomes, *Environ Microbiol*, 25, 1077-1083, 10.1111/1462-2920.16351, 2023.
- Borowski, W. S., Paull, C. K., and Ussler, W.: Marine pore-water sulfate profiles indicate in situ methane flux from underlying gas hydrate, *Geology*, 24, 655-658, 10.1130/0091-865 7613(1996)024<0655:Mpwspi>2.3.Co;2, 1996.
- Borowski, W. S., Paull, C. K., and Ussler, W.: Global and local variations of interstitial sulfate gradients in deep-water, continental margin sediments: Sensitivity to underlying methane and gas hydrates, *Marine Geology*, 159, 131-154, 10.1016/S0025-3227(99)00004-3, 1999.
- 870 Buchfink, B., Xie, C., and Huson, D. H.: Fast and sensitive protein alignment using DIAMOND, *Nat Methods*, 12, 59-60, 10.1038/nmeth.3176, 2015.
- Castresana, J.: Selection of conserved blocks from multiple alignments for their use in phylogenetic analysis, *Mol Biol Evol*, 17, 540-552, 10.1093/oxfordjournals.molbev.a026334, 2000.
- Chen, C., Wu, X., Wan, Z., Shang, J., Huang, W., Zhang, W., Liang, J., Xiao, Z., Zhou, W., and Zhong, L.: Geochemical characteristics of sediment and pore water affected by cold seeps in southern South China 875 Sea, *Frontiers in Marine Science*, 10, 10.3389/fmars.2023.1167578, 2023.
- Ciotoli, G., Procesi, M., Etiopie, G., Fracassi, U., and Ventura, G.: Influence of tectonics on global scale distribution of geological methane emissions, *Nat Commun*, 11, 2305, 10.1038/s41467-020-16229-1, 2020.

- Cline, J. D.: Spectrophotometric Determination of Hydrogen Sulfide in Natural Waters<sup>1</sup>, *Limnol Oceanogr*, 880 14, 454-458, 10.4319/lo.1969.14.3.0454, 1969.
- Cramm, M. A., Neves, B. M., Manning, C. C. M., Oldenburg, T. B. P., Archambault, P., Chakraborty, A., Cyr-Parent, A., Edinger, E. N., Jaggi, A., Mort, A., Tortell, P., and Hubert, C. R. J.: Characterization of marine microbial communities around an Arctic seabed hydrocarbon seep at Scott Inlet, Baffin Bay, *Sci Total Environ*, 762, 143961, 10.1016/j.scitotenv.2020.143961, 2021.
- 885 D'Hondt, S., Jorgensen, B. B., Miller, D. J., Batzke, A., Blake, R., Cragg, B. A., Cypionka, H., Dickens, G. R., Ferdelman, T., Hinrichs, K. U., Holm, N. G., Mitterer, R., Spivack, A., Wang, G., Bekins, B., Engelen, B., Ford, K., Gettemy, G., Rutherford, S. D., Sass, H., Skilbeck, C. G., Aiello, I. W., Guerin, G., House, C. H., Inagaki, F., Meister, P., Naehr, T., Niituma, S., Parkes, R. J., Schippers, A., Smith, D. C., Teske, A., Wiegel, J., Padilla, C. N., and Acosta, J. L.: Distributions of microbial activities in deep subseafloor 890 sediments, *Science*, 306, 2216-2221, 10.1126/science.1101155, 2004.
- Dong, X., Rattray, J. E., Campbell, D. C., Webb, J., Chakraborty, A., Adebayo, O., Matthews, S., Li, C., Fowler, M., Morrison, N. M., MacDonald, A., Groves, R. A., Lewis, I. A., Wang, S. H., Mayumi, D., Greening, C., and Hubert, C. R. J.: Thermogenic hydrocarbon biodegradation by diverse depth-stratified 895 microbial populations at a Scotian Basin cold seep, *Nat Commun*, 11, 5825, 10.1038/s41467-020-19648-2, 2020.
- Doré, A. G.: Barents Sea Geology, Petroleum Resources and Commercial Potencial, *ARCTIC*, 48, 1995.
- Edenborn, H. M., Paquin, Y., and Chateaufneuf, G.: Bacterial contribution to manganese oxidation in a deep coastal sediment, *Estuarine, Coastal and Shelf Science*, 21, 801-815, 10.1016/0272-7714(85)90074-5, 1985.
- 900 Edgar, R. C.: MUSCLE: multiple sequence alignment with high accuracy and high throughput, *Nucleic Acids Res*, 32, 1792-1797, 10.1093/nar/gkh340, 2004.
- Egger, M., Riedinger, N., Mogollón, J. M., and Jørgensen, B. B.: Global diffusive fluxes of methane in marine sediments, *Nature Geoscience*, 11, 421-425, 10.1038/s41561-018-0122-8, 2018.
- Elverhøi, A. and Solheim, A.: The Barents Sea ice sheet - a sedimentological discussion, *Polar Research*, 1, 905 23-42, 10.1111/j.1751-8369.1983.tb00729.x, 1983.
- Firriencieli, A., Negroni, A., Zanolli, G., and Cappelletti, M.: Unraveling the Metabolic Potential of Asgardarchaeota in a Sediment from the Mediterranean Hydrocarbon-Contaminated Water Basin Mar Piccolo (Taranto, Italy), *Microorganisms*, 9, 10.3390/microorganisms9040859, 2021.

- Fossing, H., Ferdelman, T. G., and Berg, P.: Sulfate reduction and methane oxidation in continental margin  
910 sediments influenced by irrigation (South-East Atlantic off Namibia), *Geochimica Et Cosmochimica Acta*, 64, 897-910, Doi 10.1016/S0016-7037(99)00349-X, 2000.
- Gabrielsen, R. H., Faersth, R. B., Jensen, L. N., Kalheim, J. E., and Riis, F.: Structural elements of the  
Norwegian continental shelf, Part 1: The Barents Sea Region, *NPD Bulletin*, 6, 1-33, 1990.
- Gouy, M., Guindon, S., and Gascuel, O.: SeaView version 4: A multiplatform graphical user interface for  
915 sequence alignment and phylogenetic tree building, *Mol Biol Evol*, 27, 221-224,  
10.1093/molbev/msp259, 2010.
- Griffith, E. M. and Paytan, A.: Barite in the ocean – occurrence, geochemistry and palaeoceanographic  
applications, *Sedimentology*, 59, 1817-1835, 10.1111/j.1365-3091.2012.01327.x, 2012.
- Guindon, S., Dufayard, J. F., Lefort, V., Anisimova, M., Hordijk, W., and Gascuel, O.: New algorithms and  
920 methods to estimate maximum-likelihood phylogenies: assessing the performance of PhyML 3.0, *Syst  
Biol*, 59, 307-321, 10.1093/sysbio/syq010, 2010.
- Guseva, N., Moiseeva, Y., Purgina, D., Gershelis, E., Yakushev, E., and Semiletov, I.: The Impact of Methane  
Seepage on the Pore-Water Geochemistry across the East Siberian Arctic Shelf, *Water*, 13,  
10.3390/w13040397, 2021.
- 925 [Hammer O, Harper D, Ryan P. PAST: Paleontological Statistics Software Package for Education and Data  
Analysis. \*Palaeont Electr.\* 2001; 4: 1–9.](#)
- Heggland, R.: Gas seepage as an indicator of deeper prospective reservoirs. A study based on exploration 3D  
seismic data, *Marine and Petroleum Geology*, 15, 1-9, 10.1016/S0264-8172(97)00060-3, 1998.
- Henrichs, S. M. and Reeburgh, W. S.: Anaerobic mineralization of marine sediment organic matter: Rates  
930 and the role of anaerobic processes in the oceanic carbon economy, *Geomicrobiology Journal*, 5, 191-  
237, 10.1080/01490458709385971, 1987.
- Hesse, R. and Schacht, U.: Early Diagenesis of Deep-Sea Sediments, in: *Deep-Sea Sediments*, edited by:  
Hüneke, H., and Mulder, T., *Developments in Sedimentology*, Elsevier, 557-713, 10.1016/b978-0-444-  
53000-4.00009-3, 2011.
- 935 Hong, W.-L., Sauer, S., Panieri, G., Ambrose, W. G., James, R. H., Plaza-Faverola, A., and Schneider, A.:  
Removal of methane through hydrological, microbial, and geochemical processes in the shallow  
sediments of pockmarks along eastern Vestnesa Ridge (Svalbard), *Limnol Oceanogr*, 61, S324-S343,  
10.1002/lno.10299, 2016.

- Hu, C.-Y., Frank Yang, T., Burr, G. S., Chuang, P.-C., Chen, H.-W., Walia, M., Chen, N.-C., Huang, Y.-C.,  
940 Lin, S., Wang, Y., Chung, S.-H., Huang, C.-D., and Chen, C.-H.: Biogeochemical cycles at the sulfate-  
methane transition zone (SMTZ) and geochemical characteristics of the pore fluids offshore southwestern  
Taiwan, *Journal of Asian Earth Sciences*, 149, 172-183, 10.1016/j.jseas.2017.07.002, 2017.
- Hunt, J. M.: *Petroleum Geochemistry and Geology*, Freeman & co, New York 1995.
- Hvoslef, S., Christie, O. H. J., Sassen, R., Kennicutt, M. C., Requejo, A. G., and Brooks, J. M.: Test of a new  
945 surface geochemistry tool for resource prediction in frontier areas, *Marine and Petroleum Geology*, 13,  
107-124, Doi 10.1016/0264-8172(95)00032-1, 1996.
- Hyatt, D., Chen, G. L., Locascio, P. F., Land, M. L., Larimer, F. W., and Hauser, L. J.: Prodigal: prokaryotic  
gene recognition and translation initiation site identification, *BMC Bioinformatics*, 11, 119,  
10.1186/1471-2105-11-119, 2010.
- 950 Iasakov, T. R., Kanapatskiy, T. A., Toshchakov, S. V., Korzhenkov, A. A., Ulyanova, M. O., and Pimenov,  
N. V.: The Baltic Sea methane pockmark microbiome: The new insights into the patterns of relative  
abundance and ANME niche separation, *Mar Environ Res*, 173, 105533,  
10.1016/j.marenvres.2021.105533, 2022.
- Iversen, N. and Jørgensen, B. B.: Anaerobic methane oxidation rates at the sulfate-methane transition in  
955 marine sediments from Kattegat and Skagerrak (Denmark)1, *Limnol Oceanogr*, 30, 944-955,  
10.4319/lo.1985.30.5.0944, 1985.
- Iversen, N. and Jørgensen, B. B.: Diffusion coefficients of sulfate and methane in marine sediments: Influence  
of porosity, *Geochemica et Cosmochemica Acta*, 57, 571-778, 10.1016/0016-7037(93)90368-7, 1993.
- Jang, J., Cao, S. C., Stern, L. A., Jung, J., and Waite, W. F.: Impact of Pore Fluid Chemistry on Fine-Grained  
960 Sediment Fabric and Compressibility, *Journal of Geophysical Research: Solid Earth*, 123, 5495-5514,  
10.1029/2018jb015872, 2018.
- Jiang, S.: *Clay Minerals from the Perspective of Oil and Gas Exploration*, in: *Clay Minerals in Nature - Their  
Characterization, Modification and Application*, 10.5772/47790, 2012.
- Johansen, S. E., Ostistiy, B. K., Birkeland, ø., Fedorovsky, Y. F., Martirosjan, V. N., Bruun Christensen, O.,  
965 Cheredeev, S. I., Ignatenko, E. A., and Margulis, L. S.: Hydrocarbon potential in the Barents Sea region:  
play distribution and potential, *Norwegian Petroleum Society Special Publications*, 2, 273-320,  
10.1016/B978-0-444-88943-0.50024-1, 1993.
- Jørgensen, B. B.: A comparison of methods for the quantification of bacterial sulfate reduction in coastal  
marine sediments, *Geomicrobiology Journal*, 1, 11-27, 10.1080/01490457809377721, 1978.

- 970 Jørgensen, B. B.: Mineralization of organic matter in the sea bed—the role of sulphate reduction, *Nature*, 296, 643-645, 10.1038/296643a0, 1982.
- Jørgensen, B. B. and Kasten, S.: Sulfur Cycling and Methane Oxidation, in: *Marine Geochemistry*, 271-309, 10.1007/3-540-32144-6\_8, 2006.
- Jørgensen, B. B., Findlay, A. J., and Pellerin, A.: The Biogeochemical Sulfur Cycle of Marine Sediments, 975 *Front Microbiol*, 10, 849, 10.3389/fmicb.2019.00849, 2019a.
- Jørgensen, B. B., Nelson, D. C., Amend, J. P., Edwards, K. J., and Lyons, T. W.: Sulfide oxidation in marine sediments: Geochemistry meets microbiology, in: *Sulfur Biogeochemistry - Past and Present*, Geological Society of America, 0, 10.1130/0-8137-2379-5.63, 2004.
- Jørgensen, B. B., Beulig, F., Egger, M., Petro, C., Scholze, C., and Røy, H.: Organoclastic sulfate reduction 980 in the sulfate-methane transition of marine sediments, *Geochimica et Cosmochimica Acta*, 254, 231-245, 10.1016/j.gca.2019.03.016, 2019b.
- Joye, S. B.: The Geology and Biogeochemistry of Hydrocarbon Seeps, *Annual Review of Earth and Planetary Sciences*, 48, 205-231, 10.1146/annurev-earth-063016-020052, 2020.
- Kallmeyer, J., Ferdelman, T. G., Weber, A., Fossing, H., and Jørgensen, B. B.: A cold chromium distillation 985 procedure for radiolabeled sulfide applied to sulfate reduction measurements, *Limnol Oceanogr-Meth*, 2, 171-180, DOI 10.4319/lom.2004.2.171, 2004.
- Kellermann, M. Y., Wegener, G., Elvert, M., Yoshinaga, M. Y., Lin, Y. S., Holler, T., Mollar, X. P., Knittel, K., and Hinrichs, K. U.: Autotrophy as a predominant mode of carbon fixation in anaerobic methane-oxidizing microbial communities, *Proc Natl Acad Sci U S A*, 109, 19321-19326, 990 10.1073/pnas.1208795109, 2012.
- [Kerr, D. E., Brown, P. J., Grey, A., and Kelleher, B. P.: The influence of organic alkalinity on the carbonate system in coastal waters, \*Marine Chemistry\*, 237, 10.1016/j.marchem.2021.104050, 2021.](#)
- Kim, J., Dong, H. L., Seabaugh, J., Newell, S. W., and Eberl, D. D.: Role of microbes in the smectite-to-illite reaction, *Science*, 303, 830-832, DOI 10.1126/science.1093245, 2004.
- 995 Kleindienst, S., Herbst, F. A., Stagars, M., von Netzer, F., von Bergen, M., Seifert, J., Peplies, J., Amann, R., Musat, F., Lueders, T., and Knittel, K.: Diverse sulfate-reducing bacteria of the *Desulfosarcina/Desulfococcus* clade are the key alkane degraders at marine seeps, *ISME J*, 8, 2029-2044, 10.1038/ismej.2014.51, 2014.

- Knies, J. and Martinez, P.: Organic matter sedimentation in the western Barents Sea region: Terrestrial and  
1000 marine contribution based on isotopic composition and organic nitrogen content, *Norwegian Journal of  
Geology*, 89, 79-89, 2009.
- [Knittel, K., Wegener, G., and Boetius, A.: Anaerobic Methane Oxidizers, in: Microbial Communities  
Utilizing Hydrocarbons and Lipids: Members, Metagenomics and Ecophysiology, 1-21, 10.1007/978-3-  
319-60063-5\\_7-1, 2018.](#)
- 1005 Larssen, G. B., Elvebakk, G., Henriksen, L. B., Kristensen, S.-E., Nilsson, I., Samuelsen, T. J., Svana, T.  
A., Stemmerik, L., and Worsley, D.: Upper Palaeozoic lithostratigraphy of the Southern Norwegian  
Barents Sea, in, 2002.
- Li, H. and Durbin, R.: Fast and accurate short read alignment with Burrows-Wheeler transform,  
*Bioinformatics*, 25, 1754-1760, 10.1093/bioinformatics/btp324, 2009.
- 1010 Liao, Y., Smyth, G. K., and Shi, W.: featureCounts: an efficient general purpose program for assigning  
sequence reads to genomic features, *Bioinformatics*, 30, 923-930, 10.1093/bioinformatics/btt656, 2014.
- MacLeod, F., Kindler, G. S., Wong, H. L., Chen, R., and Burns, B. P.: Asgard archaea: Diversity, function,  
and evolutionary implications in a range of microbiomes, *AIMS Microbiol.*, 5, 48-61,  
10.3934/microbiol.2019.1.48, 2019.
- 1015 Martens, C. S. and Berner, R. A.: Methane production in the interstitial waters of sulfate-depleted marine  
sediments, *Science*, 185, 1167-1169, 10.1126/science.185.4157.1167, 1974.
- Middelburg, J. J.: Reviews and syntheses: to the bottom of carbon processing at the seafloor, *Biogeosciences*,  
15, 413-427, 10.5194/bg-15-413-2018, 2018.
- Mölder, F., Jablonski, K. P., Letcher, B., Hall, M. B., Tomkins-Tinch, C. H., Sochat, V., Forster, J., Lee, S.,  
1020 Twardziok, S. O., Kanitz, A., Wilm, A., Holtgrewe, M., Rahmann, S., Nahnsen, S., and Koster, J.:  
Sustainable data analysis with Snakemake, *F1000Res*, 10, 33, 10.12688/f1000research.29032.2, 2021.
- Nickel, J. C., di Primio, R., Mangelsdorf, K., Stoddart, D., and Kallmeyer, J.: Characterization of microbial  
activity in pockmark fields of the SW-Barents Sea, *Marine Geology*, 332-334, 152-162,  
10.1016/j.margeo.2012.02.002, 2012.
- 1025 Nickel, J. C., di Primio, R., Kallmeyer, J., Hammer, Ø., Horsfield, B., Stoddart, D., Brunstad, H., and  
Mangelsdorf, K.: Tracing the origin of thermogenic hydrocarbon signals in pockmarks from the  
southwestern Barents Sea, *Organic Geochemistry*, 63, 73-84, 10.1016/j.orggeochem.2013.08.008, 2013.

- Nunoura, T., Soffientino, B., Blazejak, A., Kakuta, J., Oida, H., Schippers, A., and Takai, K.: Subseafloor microbial communities associated with rapid turbidite deposition in the Gulf of Mexico continental slope (IODP Expedition 308), *FEMS Microbiol Ecol*, 69, 410-424, 10.1111/j.1574-6941.2009.00718.x, 2009.
- 1030 Parkes, R. J., Cragg, B., Roussel, E., Webster, G., Weightman, A., and Sass, H.: A review of prokaryotic populations and processes in sub-seafloor sediments, including biosphere:geosphere interactions, *Marine Geology*, 352, 409-425, 10.1016/j.margeo.2014.02.009, 2014.
- Pellerin, A., Bui, T. H., Rough, M., Mucci, A., Canfield, D. E., and Wing, B. A.: Mass-dependent sulfur isotope fractionation during reoxidative sulfur cycling: A case study from Mangrove Lake, Bermuda, *Geochimica et Cosmochimica Acta*, 149, 152-164, 10.1016/j.gca.2014.11.007, 2015.
- 1035 Pop Ristova, P., Wenzhofer, F., Ramette, A., Felden, J., and Boetius, A.: Spatial scales of bacterial community diversity at cold seeps (Eastern Mediterranean Sea), *ISME J*, 9, 1306-1318, 10.1038/ismej.2014.217, 2015.
- 1040 Raab, A. and Feldmann, J.: Microbial transformation of metals and metalloids, *Sci Prog*, 86, 179-202, 10.3184/003685003783238671, 2003.
- Rasheed, M. A., Lakshmi, M., Rao, P. L. S., Kalpana, M. S., Dayal, A. M., and Patil, D. J.: Geochemical evidences of trace metal anomalies for finding hydrocarbon microseepage in the petroliferous regions of the Tatipaka and Pasarlapudi areas of Krishna Godavari Basin, India, *Petroleum Science*, 10, 19-29, 10.1007/s12182-013-0245-x, 2013.
- 1045 Rovere, M., Mercorella, A., Frapiccini, E., Funari, V., Spagnoli, F., Pellegrini, C., Bonetti, A. S., Veneruso, T., Tassetti, A. N., Dell'Orso, M., Mastroianni, M., Giuliani, G., De Marco, R., Fabi, G., Ciccone, F., and Antoncecchi, I.: Geochemical and Geophysical Monitoring of Hydrocarbon Seepage in the Adriatic Sea, *Sensors (Basel)*, 20, 10.3390/s20051504, 2020.
- 1050 Ruff, S. E., Biddle, J. F., Teske, A. P., Knittel, K., Boetius, A., and Ramette, A.: Global dispersion and local diversification of the methane seep microbiome, *Proc Natl Acad Sci U S A*, 112, 4015-4020, 10.1073/pnas.1421865112, 2015.
- [Ruiz-Blas F., Bartholomäus A., Yang S., Wagner D., Henny C., Russell J. M., Kallmeyer J., and Vuillemin A. Metabolic features that select for Bathyarchaeia in modern ferruginous lacustrine subsurface sediments. ISME Communications, in press. 10.1093/ismeco/ycae112, 2024](#)
- 1055 Sættem, J., Rise, L., and Westgaard, D. A.: Composition and properties of glacial sediments in the southwestern Barents Sea, *Marine Geotechnology*, 10, 229-255, 10.1080/10641199109379893, 1991.

hat gelöscht: ¶



- Schulz, H. D.: Quantification of Early Diagenesis: Dissolved Constituents in Pore Water and Signals in the Solid Phase, in: *Marine Geochemistry*, 73-124, 10.1007/3-540-32144-6\_3, 2006.
- 1060 Schwengers, O., Jelonek, L., Dieckmann, M. A., Beyvers, S., Blom, J., and Goesmann, A.: Bakta: rapid and standardized annotation of bacterial genomes via alignment-free sequence identification, *Microb Genom*, 7, 10.1099/mgen.0.000685, 2021.
- Seeberg-Elverfeldt, J., Schluter, M., Feseker, T., and Kolling, M.: Rhizon sampling of porewaters near the sediment-water interface of aquatic systems, *Limnol Oceanogr-Meth*, 3, 361-371, 10.4319/lom.2005.3.361, 2005.
- 1065 Sultan, N., Garziglia, S., and Ruffine, L.: New insights into the transport processes controlling the sulfate-methane-transition-zone near methane vents, *Sci Rep*, 6, 26701, 10.1038/srep26701, 2016.
- Teske, A.: Hydrocarbon-Degrading Microbial Communities in Natural Oil Seeps, in: *Microbial Communities Utilizing Hydrocarbons and Lipids: Members, Metagenomics and Ecophysiology*, 1-31, 10.1007/978-3-319-60063-5\_3-2, 2019.
- 1070 Turchyn, A. V., Bradbury, H. J., Walker, K., and Sun, X.: Controls on the Precipitation of Carbonate Minerals Within Marine Sediments, *Frontiers in Earth Science*, 9, 10.3389/feart.2021.618311, 2021.
- Vuillemin, A., Kerrigan, Z., D'Hondt, S., and Orsi, W. D.: Exploring the abundance, metabolic potential and gene expression of seafloor Chloroflexi in million-year-old oxic and anoxic abyssal clay, *FEMS Microbiol Ecol*, 96, 10.1093/femsec/fiaa223, 2020a.
- 1075 Vuillemin, A., Vargas, S., Coskun, O. K., Pockalny, R., Murray, R. W., Smith, D. C., D'Hondt, S., and Orsi, W. D.: Atribacteria Reproducing over Millions of Years in the Atlantic Abyssal Subseafloor, *mBio*, 11, 10.1128/mBio.01937-20, 2020b.
- 1080 [Vuillemin A., Coskun O. K., and Orsi W. D.: Microbial activities and selection from surface ocean to subseafloor on the Namibian continental shelf, \*Applied and Environmental Microbiology\*, 88, e00216-22, 0.1128/aem.00216-22, 2022.](#)
- [Wegener, G., Laso-Perez, R., Orphan, V. J., and Boetius, A.: Anaerobic Degradation of Alkanes by Marine Archaea, \*Annu Rev Microbiol\*, 76, 553-577, 10.1146/annurev-micro-111021-045911, 2022.](#)
- 1085 [Widdel, F., Knittel, K., and Galushko, A.: Anaerobic Hydrocarbon- Degrading Microorganisms: An Overview, in: \*Handbook of Hydrocarbon and Lipid Microbiology\*, Springer, Berlin, Heidelberg, 1997-2021, <https://doi.org/10.1007/978-3-540-77587-4>, 2010.](#)
- Yergin, D.: *The Prize: The Epic Quest for Oil, Money & Power*, Free Press 2009.

hat gelöscht: ¶

1090 Zhang, C., Fang, Y. X., Yin, X., Lai, H., Kuang, Z., Zhang, T., Xu, X. P., Wegener, G., Wang, J. H., and Dong, X.: The majority of microorganisms in gas hydrate-bearing seafloor sediments ferment macromolecules, *Microbiome*, 11, 37, 10.1186/s40168-023-01482-5, 2023.

[Zhang, C. J., Zhou, Z., Cha, G., Li, L., Fu, L., Liu, L. Y., Yang, L., Wegener, G., Cheng, L., and Li, M.: Anaerobic hydrocarbon biodegradation by alkylotrophic methanogens in deep oil reservoirs, \*ISME J\*, 18, 10.1093/ismejo/wrae152, 2024.](#)

1095 [Zhou, Z., Zhang, C.-j., Liu, P.-f., Fu, L., Laso-Pérez, R., Yang, L., Bai, L.-p., Li, J., Yang, M., Lin, J.-z., Wang, W.-d., Wegener, G., Li, M., and Cheng, L.: Non-syntrophic methanogenic hydrocarbon degradation by an archaeal species, \*Nature\*, 601, 257-262, 10.1038/s41586-021-04235-2, 2021.](#)

1100